AIAA 2004-1529

Multi-Configuration Space Frames

T. Schioler and S. Pellegrino
University of Cambridge, Cambridge, CB2 1PZ, UK

45th AIAA/ASME/ASCE/AHS/ASC Structures, Structural Dynamics, and Materials Conference
19-22 April 2004
Palm Springs, CA

Multi-Configuration Space Frames

T. Schioler* and S. Pellegrino†
University of Cambridge, Cambridge, CB2 1PZ, UK

This paper is concerned with the design of beam-like or surface-like structures for use, for example, as large spacecraft antennae, or as reconfigurable partitions in buildings that control air flow or sound. The idea is to construct structures that include a large number of bi-stable elements, and to exploit the two states of each actuator to set up different configurations of the structure. By increasing the number of actuators, structures with a large number of different configurations can be designed. A particular attraction of this approach is that it produces structures able to maintain their shape in a power-off state. The first part of this paper focuses on the design and realization of a low-cost snap-through strut, whose two different lengths provide the required bi-stable feature. A parametric study of the length-change of the strut in relation to the peak force that needs to be applied by the driving actuators is carried out. Bi-stable struts based on this concept have been made by injection moulding Nylon. Next, beam-like structures based on different architectures are considered. It is shown that different structural architectures produce structures with workspaces of different size and resolution when made from an identical number of bi-stable struts. One particular architecture, with 30 bi-stable struts and hence over 1 billion different configurations, has been demonstrated.

Introduction and Background

A requirement that is common to many fields of engineering is the need for low cost, reliable, reconfigurable structures. Potential applications include robotic manipulator arms, surfaces that control ventilation in buildings and active facades that control the sunlight entering a building. Additionally, there are applications involving radioactive or toxic environments where it may be cheaper to use low cost disposable manipulators than high cost manipulators that have to be decontaminated after use.

Focussing, for example, on robotic manipulators, the relatively high cost of traditional devices results from the use of continuous actuation and the ancillary need for feedback control systems. A novel approach to these requirements is to combine two known structural concepts: a variable geometry truss and a bistable structural element.

Variable geometry trusses (VGTs) were first introduced in the context of crane-like devices that could be used to help build large space stations or Mars exploration vehicles in orbit [1, 2]. A VGT is a three-dimensional assembly of struts connected only at the ends (hence a *truss* structure), whose configuration is determined by the length of the struts. In order for the configuration of the structure to be *uniquely* determined by the lengths of the struts, kinematically determinate architectures are adopted. Similarly, statically determinate architectures are adopted in order to ensure that any change in length of the struts does not induce stresses in the structure. I.e. the structure does not fight against the imposed change in length of the strut [3].

The idea of using bistable structural elements in robotic devices was proposed quite some time ago [4,5]. Further work has been done in the area in the last ten years, especially at MIT [6–8] and Johns Hopkins University [9–11]. As has been recognised by previous researchers, if the number of bistable elements in a VGT is large enough, the freedom of movement of the truss approaches that of a system with continuous actuators. However, the control requirements for the binary VGT would be much simpler, as the current configuration of the structure would be determined simply by the state of its bistable elements.

The majority of the work done at JHU has been focused on the macroscopic control of VGTs such as forward and inverse kinematics. Prototype trusses have been built using pneumatic actuators as bistable elements. Related work has been done by Professor Dubowsky's group at MIT. Additionally, however, the MIT group have pioneered the use of Electrostrictive Polymer Artificial Muscles (EPAM) actuators. Compared to pneumatic actuators, EPAMs have the prospect of being cheaper and lighter, as well as circumventing the requirement for compressed air lines. Following on from this work, our approach relies on a novel and very simple, ultra low-cost snap-through strut, whose behaviour can easily be tuned to be highly repeatable.

This paper consists of two parts. The first part focuses on the design and realization of a low-cost snap-through strut, whose two different lengths provide the required bi-stable feature. A parametric study of the change in length (i.e. the stroke) of the strut in

*Research Student, Department of Engineering, Trumpington Street.
†Professor of Structural Engineering, Department of Engineering, Trumpington Street. Associate Fellow AIAA. pellegrino@eng.cam.ac.uk

relation to the peak force that needs to be applied by the driving actuators is carried out. Bi-stable struts based on this concept have been made by injection moulding Nylon.

In the second part, beam-like structures based on different VGT architectures are considered. It is shown that different structural architectures produce structures with workspaces of different size and resolution when made from an identical number of bi-stable struts. The only actuation that is required is to flip the struts in between their two states. One particular architecture, with 30 bi-stable struts and hence around 10^9 different configurations, is demonstrated.

Mises Truss

The bistable snap-through strut considered in this paper is based on the Mises truss shown in Figure 1(a). The Mises truss is a three-pin-arch constructed from two struts of equal length. It is a well-known structure that has been investigated extensively [12, 13]. When a central vertical force, $2F$, is applied at the apex as shown, the struts deform axially according to their stiffness. The deformation is symmetric and can be analysed by considering only half of the structure, see Figure 1(b).

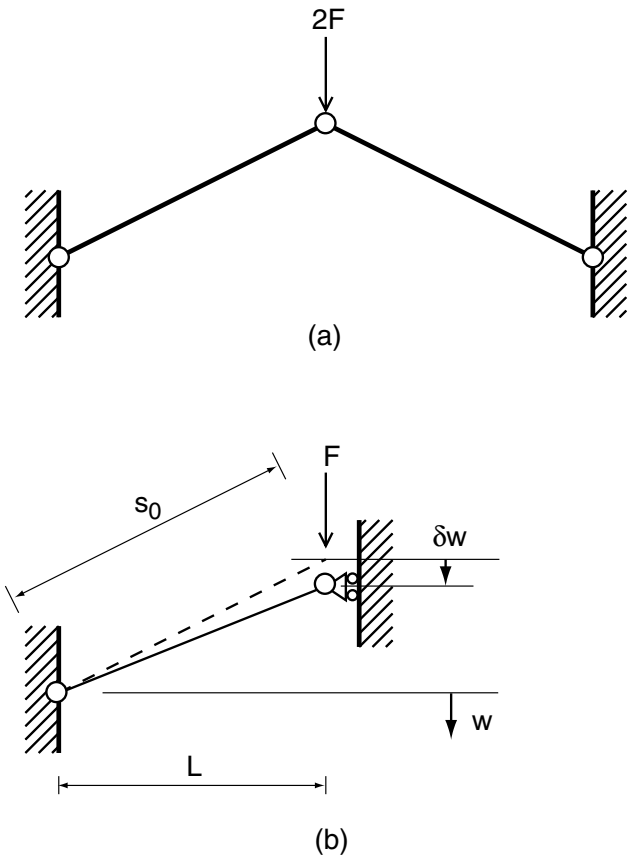

Fig. 1 Mises truss

Assuming that the struts remain straight and linear-elastic, in any configuration the axial force in each strut, P, is given by its length decrease, δs, divided by its initial length, s_0, multiplied by the axial stiffness of the strut

$$P = EA\frac{\delta s}{s_0} \tag{1}$$

where P is positive in compression. Therefore,

$$F = -P\frac{w}{\sqrt{w^2 + L^2}} \tag{2}$$

By plotting F versus (w/w_0), Figure 2, we can see that this truss has stable equilibria under $F = 0$ at $w = \pm w_0$, and a physically unrealizable, unstable equilibrium at $w = 0$.

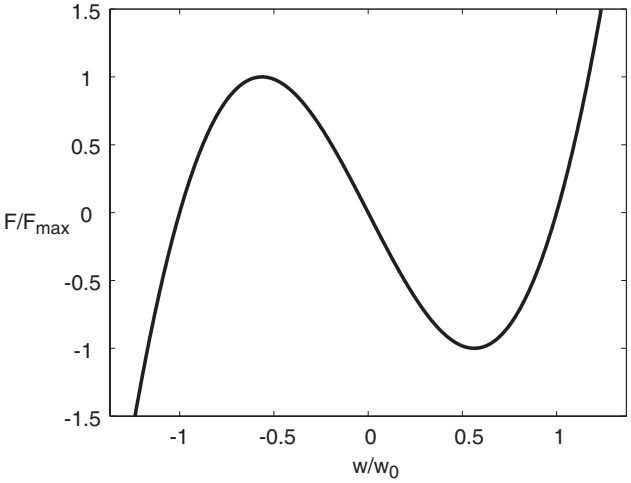

Fig. 2 Force versus rise of a typical Mises Truss.

This means that the Mises truss is a bistable structure. Moreover, if the movement of the truss is force-controlled, it will behave in a snap-through manner. For example, examine the case where an increasing downwards force is applied to a truss with an initially positive value of w, which is the configuration shown in Figure 1(a). The truss will deform according to Figure 2. When the maximum compressive force has been reached, the truss will snap through till it can support the downwards force through tension in the struts.

Snap-Through Strut

Geometry

A bistable structure with the same snap-through behaviour as the Mises truss is shown in Figure 3. The idea is to use a pair of identical Mises trusses, which provide the required snapping behaviour, to connect two stiff elements, AG and CFHE. The reason why a pair of Mises trusses is used, is that if only one truss was used the element AG would be free to rotate in plane. Out-of-plane bending stiffness is imparted to the structure by giving it some depth, which means that the pin-jointed connections shown in the diagram are in fact revolute joints, which in three dimensions

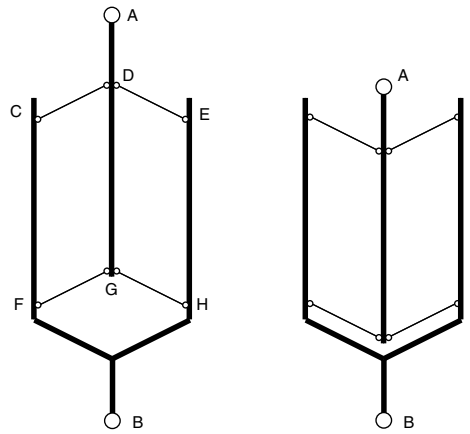

Fig. 3 Concept of snap-through strut.

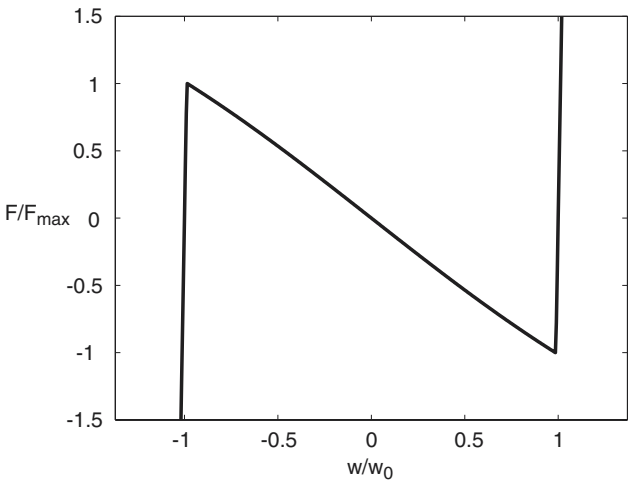

Fig. 4 Behaviour of a typical Mises truss, whose elements are allowed to buckle.

allow only a one-degree-of-freedom rotation about an axis orthogonal to the plane of the diagram.

Snap-through struts designed such that they follow the classical Mises truss behaviour, i.e. the elements CD, DE, etc. do not buckle, have the disadvantage that their overall axial stiffness will be relatively small in comparison with the force at which they snap through. This follows from the smooth non-linear F vs. w response shown in Figure 2. Another disadvantage is that only relatively small values w_0 can be accommodated without yielding the material, and so the *s*troke of the strut, $2w_0$, is rather limited.

An alternative is to design struts with much larger values of $2w_0$, whose elements buckle elastically. Such struts will snap by *bifurcation buckling* instead of reaching a *limit point*, and their design involves considering the Euler buckling load of the inclined elements. This approach affords much greater freedom to the designer, and allows the snap-through load of a relatively stiff Mises truss to be reduced to the required level. A typical Force vs. Displacement plot for a Mises truss whose members are allowed to buckle as classical Euler struts is shown in Figure 4.

Another solution is to insert stops that limit the travel of the moving element AG. This has the advantage of conferring higher stiffness at the cost of some complexity in the design, and a reduction in the stroke of the bistable strut.

Maximum Force

In most practical designs of snap-through struts, the inclined elements CD, DE, etc. almost invariably buckle relatively early on. This means that a very simple analytical model can be used to predict the maximum force that can be supported by a snap-through strut before it actually snaps through. The maximum axial force in the members CD, DE, FG, GH is their Euler buckling load P_E

$$P_{max} = P_E = \frac{\pi^2 EI}{s_0^2} \tag{3}$$

The overall vertical force, F_{max}, corresponding to only one inclined element, as shown in Figure 1(b) is equal to the vertical component of this force. Therefore,

$$F_{max} = P_E \frac{w}{s} \tag{4}$$

If the assumption is made that the vertical movement of the apex joint before buckling is negligible, then $s \approx s_0$ and $w \approx w_0$, which makes the calculation of F_{max} very simple. Assuming the inclined elements to have rectangular cross-section of height t and breadth b

$$F_{max} = \frac{\pi^2 Ebt^3}{12s^2}\frac{w_0}{s} \tag{5}$$

$$= \frac{\pi^2 Ebt^3}{12}\frac{w_0}{(w_0^2+L^2)^{\frac{3}{2}}} \tag{6}$$

To find the maximum possible value of F_{max} for any given material and strut thickness, consider

$$\frac{dF_{max}}{dw_0} = \frac{\pi^2 Ebt^3}{12}\frac{(w_0^2+L^2)^{\frac{3}{2}} - 3w_0^2(w_0^2+L^2)^{\frac{1}{2}}}{(w_0^2+L^2)^3} \tag{7}$$

Setting Equation 7 equal to zero gives

$$(w_0^2+L^2)^{\frac{3}{2}} = 3w_0^2(w_0^2+L^2)^{\frac{1}{2}} \tag{8}$$

from which

$$w_0 = L/\sqrt{2} \tag{9}$$

Substitute this value of w into Equation 4 to obtain the maximum possible value of F_{max}

$$\text{Max}(F_{max}) = \frac{\pi^2 Ebt^3}{12}\frac{\sqrt{\frac{1}{2}}L}{(\frac{1}{2}L^2+L^2)^{\frac{3}{2}}}$$

$$= \frac{\pi^2}{18\sqrt{3}}\frac{Ebt^3}{L^2} \tag{10}$$

It is useful for design purposes to plot $F_{max}/\mathrm{Max}(F_{max})$, given by ratio between Equation 6 and Equation 10 against w_0/L. See Figure 5.

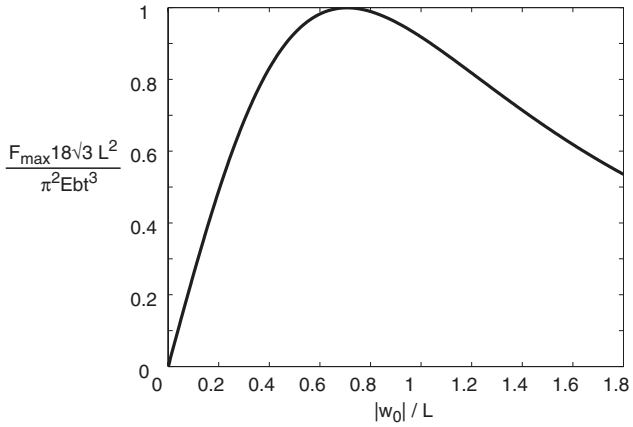

Fig. 5 Variation of snapping force, assuming inextensional behaviour.

The above analysis can be refined to include the elastic shortening of the inclined elements, but this time the resulting solution has to be solved iteratively. The results, for various values of t/L, have been plotted in Figure 6. This figure shows that for high values of w_0/L, inclined elements with t/L up to 0.1 still approximate closely to inextensional elements for the purpose of estimating F_{max}. At lower values of w_0/L the approximation is less good and an analysis considering the extension of these elements is required to get an accurate estimate for F_{max}.

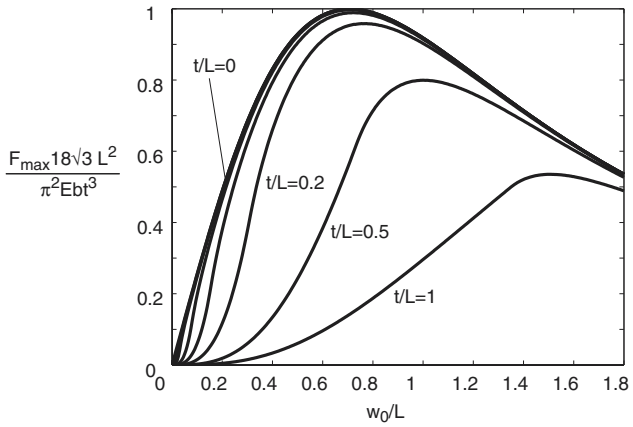

Fig. 6 Variation of snapping force, accounting for extensional behaviour.

Constraints due to Yield Strain

It is also necessary to ensure that the maximum strains induced in the structural members remain lower than the yield strain of the material.

For any design of the strut, the maximum strain occurs when the ends of the inclined elements are closest, hence when $w = 0$ as shown in Figure 7. Assuming the

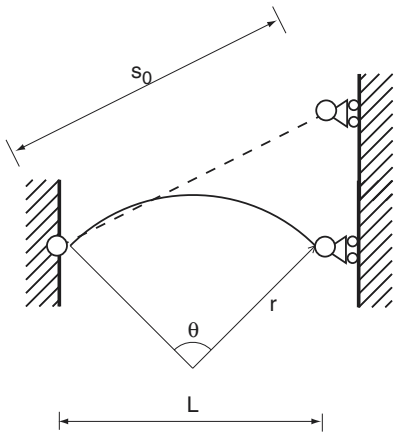

Fig. 7 Configuration of maximum strain.

inclined elements to be slender, the strains along the centre line can be neglected in comparison with the maximum bending strains. These can be calculated as follows

$$L = 2r \sin\frac{\theta}{2} = 2r \sin\frac{s_0}{2r} \tag{11}$$

also,

$$\varepsilon = \frac{t}{2r} \tag{12}$$

Rearranging Equation 11 gives

$$r = \frac{L}{2} / \sin\frac{S}{2r} \tag{13}$$

which can be solved iteratively to find r for any given value of L and w_0. Once r is known, ε can be found using Equation 12. Figure 8 shows a plot of ε against w_0.

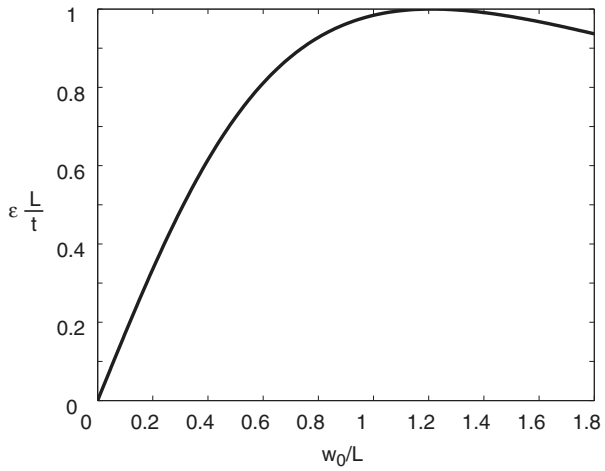

Fig. 8 Maximum bending strain during snap through.

As can be seen, the maximum strain is reached when $w_0 = 1.211L$. This corresponds to the case where the

inclined elements take up a a semi-circular shape when $w = 0$, hence in Figure 7 $\theta = \pi$, $L = 2r$ and $s_0 = \pi r$

$$w_0 = \sqrt{s_0^2 - L^2} = r\sqrt{\pi^2 - 4} \approx 1.211L \qquad (14)$$

When ε has been evaluated, dividing F_{max} by ε in their non-dimensional forms and plotting this against w_0 produces the plot in Figure 9. This plot shows that on a force-per-unit-strain basis, low values of w_0/L are preferable.

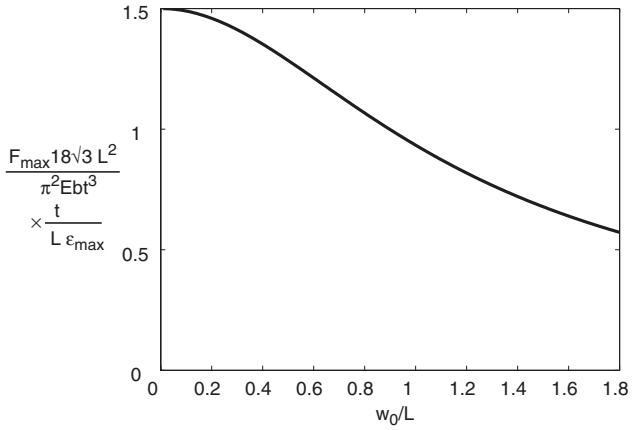

Fig. 9 Variation of F_{max}/ε with w_0.

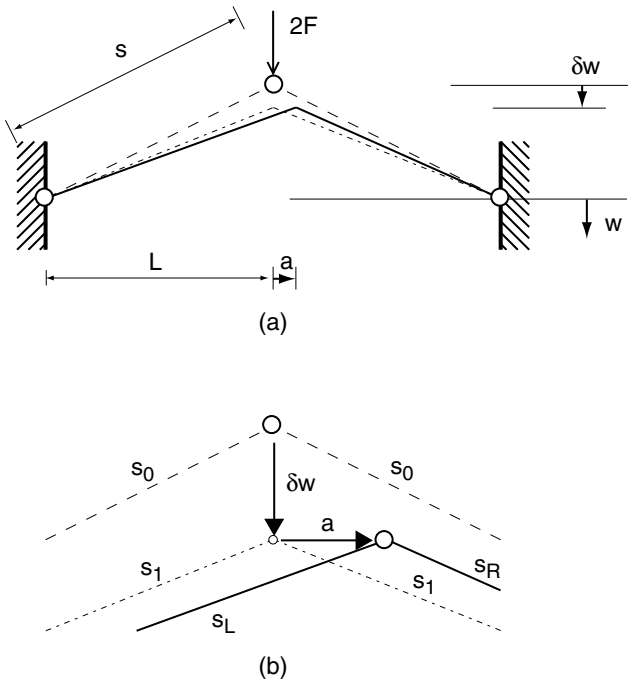

Fig. 10 Geometry of a Mises truss behaving in an asymmetric manner.

Asymmetric Buckling

All of the analyses presented above have assumed that the Mises trusses that make up the snap-through strut buckle symmetrically. Although the snap-through of the classical Mises truss —whose members do not themselves buckle— is symmetric, it is not obvious that this is still the case when the members are allowed to buckle. In order to ascertain whether or not the buckling would be symmetric, the following analysis was done.

Consider the situation shown in Figure 10, where the apex of a Mises truss consisting of two identical members of initial length s_0 has moved downwards by δw and horizontally by a.

Because the two members can be either in buckled or unbuckled states, the horizontal force components in the left and right inclined members are given by

$$\begin{aligned} H_L &= \frac{EA}{L}(s_L - s_0)\frac{L+a}{s_L} \text{ if } \frac{EA}{L}(s_L - s_0) < P_E \\ &= P_E\frac{L+a}{s_L} \text{ otherwise} \end{aligned} \qquad (15)$$

and

$$\begin{aligned} H_R &= \frac{EA}{L}(s_R - s_0)\frac{L-a}{s_R} \text{ if } \frac{EA}{L}(s_R - s_0) < P_E \\ &= P_E\frac{L-a}{s_R} \text{ otherwise} \end{aligned} \qquad (16)$$

where s_L and s_R are the current lengths of the left and right inclined members, respectively.

The variation of these two forces with the lateral displacement a has been plotted in Figure 11 for the case $L = 10$ mm, $w_0 = 3.25$ mm, $\delta w = 0$ mm and $P_E = 10$ N. However, the main features that can be noted from this figure are quite general. When $a < -0.32$, only the left strut is buckled. When $a > 0.32$, only the right strut is buckled. When $-0.32 < a < 0.32$ both the struts are buckled. Regardless of the specific numbers, it can be noted that the curves are very steep when the struts are unbuckled, but become practically horizontal when P_E is reached. In fact, the horizontal stiffness is negative due to changes in geometry.

It is clear from this plot that there are three equilibrium points, where the curves cross. The left and right equilibrium points are stable, whereas the centre one is unstable. This means that the symmetric configuration, in which $a = 0$, is not stable. The stable configurations are when one strut is straight and the other is buckled.

Having established that, once one or both of its inclined members have buckled, the Mises truss does not behave symmetrically, it seems sensible to establish whether or not this has any effect on F_{max}. Three methods were employed to investigate whether or not this is the case. The first was a standard analytical buckling analysis. The second was an eigenvalue analysis conducted using ABAQUS. The last analysis was a static FE analysis, again done using ABAQUS.

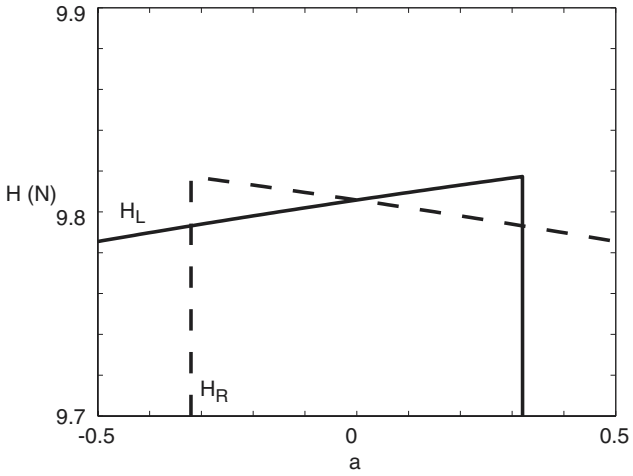

Fig. 11 Variation of horizontal force components during asymmetric buckling of Mises truss.

Analytical Buckling Analysis

Buckling will only occur once the axial force in one or other of the struts is equal to the Euler buckling load. In order to determine whether or not an incipient buckling mode will be symmetric or asymmetric, we will look at the changes in strain energy in the structure as it buckles symmetrically or asymmetrically. In both cases the vertical load $2F$ is such that the axial forces in at least one of the struts is exactly equal to P_E.

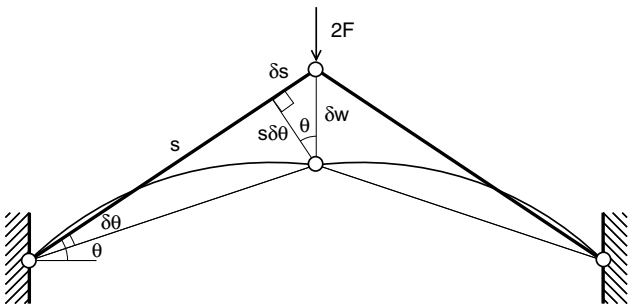

Fig. 12 Symmetric buckling of a Mises truss.

Figure 12 shows a schematic diagram of a Mises truss buckling in a symmetric manner. The work done by the external force $2F$ is

$$\Delta W = 2F\delta w \tag{17}$$

The change in strain energy as the structure buckles symmetrically is

$$\Delta W = 2P_E\delta s \tag{18}$$

where

$$\delta s = \delta w \sin\theta \tag{19}$$

Combining these two equations gives

$$F = P_E \sin\theta \tag{20}$$

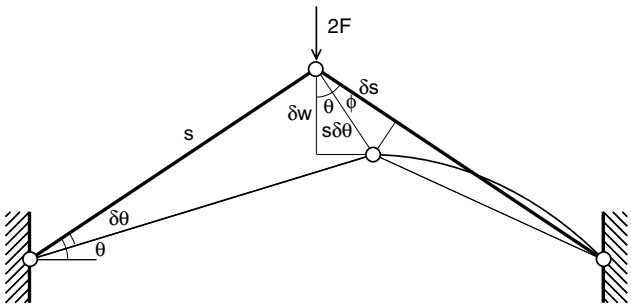

Fig. 13 Asymmetric buckling of a Mises truss.

Similarly, Figure 13 shows a Mises truss buckling asymmetrically. Here the left strut remains unbuckled, as suggested by the plot of horizontal forces in Figure 11, and so the change in strain energy is

$$\Delta W = P_E\delta s \tag{21}$$

In this case, however,

$$\delta s = \frac{\delta w}{\cos\theta}\cos\phi \tag{22}$$

Therefore, substituting Equation 22 into Equation 21 gives

$$\Delta W = P_E\delta w\frac{sin2\theta}{cos\theta} \tag{23}$$

But, since

$$\phi = \frac{\pi}{2} - 2\theta \tag{24}$$

$$\cos\phi = \sin(2\theta) \tag{25}$$

Equation 23 and Equation 17 become

$$F = P_E \sin\theta \tag{26}$$

In conclusion, from an energy perspective, there is no preference for asymmetric buckling at the point where $F = F_{max}$.

Finite Element Analyses

Two different sets of finite element analyses were completed using the commercial package ABAQUS. In both cases, the structure analysed was a Mises truss with the characteristics listed in Table 1.

Symbol	Description	Value
b	Width of plate	5 mm
E	Young's Modulus	210,000 N/mm^2
L	Half span	10 mm
t	Plate thickness	0.05 mm
w_0	Rise of truss	2 mm

Table 1 Properties of Mises truss for FE analysis.

The first set of analyses involved calculating the symmetric and asymmetric eigenvalues for the structure. This was done both on the unloaded truss and

on a truss that had been preloaded with $F_{preload} = 0.985\ F_{max}$. The buckling modes obtained thus are shown in Figures 14 to 17. As can be seen, the symmetric and asymmetric buckling modes are very similar regardless of preload. The eigenvalues of the preloaded trusses are the load increment that needs to be applied for the structure to buckle, hence their values are much lower than for the unloaded structure. However, when the total load is considered, see Table 2, there is practically no difference.

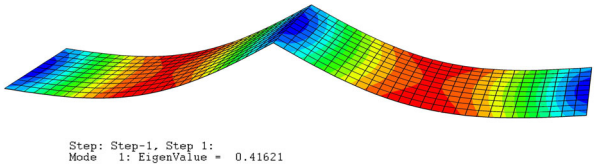

Fig. 14 First symmetric eigenvector.

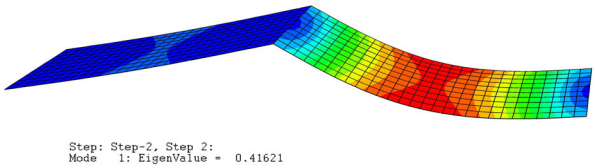

Fig. 15 First asymmetric eigenvector.

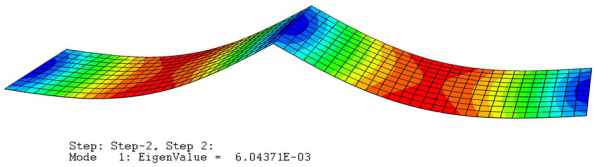

Fig. 16 First symmetric eigenvector of preloaded structure.

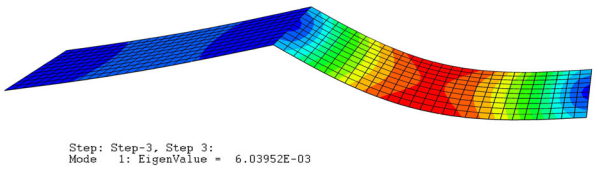

Fig. 17 First asymmetric eigenvector of preloaded structure.

The second set of FE analyses were general non-linear analyses that examined the maximum vertical force supported by the truss as the center was forced downwards. In both cases, small initial imperfections were introduced to ensure that the plates deformed by bending rather than by axial shortening. These imperfections were introduced by applying small transverse loads at the centre of each plate before imposing the vertical deflection of the apex.

In the first analysis, the imperfections applied were symmetric and the centre of the truss was not allowed to move horizontally. This produced a symmetric buckling pattern. In the second analysis, the applied imperfections were asymmetric and horizontal movement of the centre of the truss was permitted. This produced an asymmetric buckling pattern. The values of the maximum supported loads in each case can be seen in Table 2.

Buckling Load $2F$ (N)	Analysis Method
0.4052	Euler buckling of plates
0.41621	Symmetric eigenvector (no preload)
0.41621	Asymmetric eigenvector (no preload)
0.41604	Symmetric eigenvector (preload)
0.41604	Asymmetric eigenvector (no preload)
0.415244	Symmetric non-linear
0.410409	Asymmetric non-linear

Table 2 Buckling loads comparison for truss described in Table 1.

As can be seen, all of these values are very similar, which suggests that the simple analytical method that bases its predictions on elastic axial shortening, Euler buckling and symmetric behaviour will give good predictions. The axial compression of the plates prior to buckling also explains why the eigenvector analysis without preload gives slightly higher estimates than that with preload. Lastly, it can be seen that although the structure has a slight preference for asymmetric behaviour, the difference in F_{max} is negligible.

Realisation of Strut

Having extensively analysed the snap-through strut it was decided to manufacture a working prototype. The material selection was governed by the requirement for a relatively large stroke relative to the overall length of the strut. This called for a material with high yield strain. High yield strain was also a requirement for the elastic hinges that would connect the plates to the central vertical element and the sides.

A suitable material is Nylon 6, which has the attraction of being relatively easy to form into reliable elastic hinges. Having decided on Nylon, a natural choice for the manufacturing technique was injection moulding. Figure 18 shows a sketch of the manufactured design. The characteristics of this strut are set out in Table 3. Note that in this particular implementation the strut has a stroke of about 5 mm, corresponding to about 10% of its overall length.

Figure 19 shows a prototype. Note the horizontal "straps", not shown in Figure 18, that connect the side members. These members prevent lateral movement of the side walls when the inclined elements are placed under compression. If these members were not present, the side members would simply bend outwards and there would be hardly any snap-through behaviour.

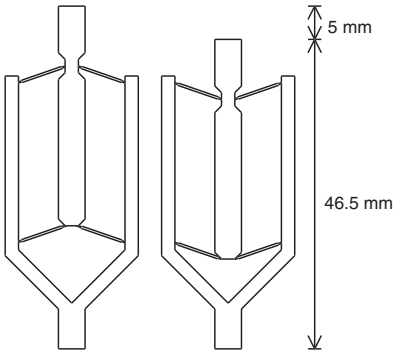

Fig. 18 Sketch of bistable strut.

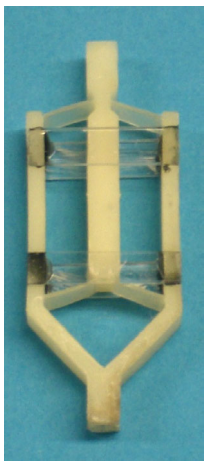

Fig. 19 A prototype bistable strut.

Experimental Results

Having manufactured a working bistable strut, this was then tested in an Instron materials testing machine. Figure 20 shows the measured force-displacement characteristics as well as the theoretical response derived by assuming elastic axial shortening and Euler buckling. The solid line represents the theoretical prediction. The upper dotted line shows the data recorded as the strut is being compressed, the lower dotted line corresponds to the strut being extended.

As can be seen, the analytical model gives quite good results. The errors can be explained by the fact that Nylon is neither linear nor perfectly elastic. Furthermore, there is some friction between the central post and the horizontal bracing elements. All of these factors lead one to expect a certain amount of hysteresis in the response. It is however clear that the strut does indeed have two stable points and if moved from either will attempt to return to one or the other.

Symbol	Description	Value
b	Width of plate	5 mm
E	Young's Modulus	3,000 N/mm^2
L	Half span of truss	7 mm
t	Plate thickness	0.35 mm
w_0	Rise of truss	2 mm
-	Length of hinge section	0.4 mm
-	Thickness of hinge section	0.15 mm

Table 3 Snap-through strut prototype characteristics.

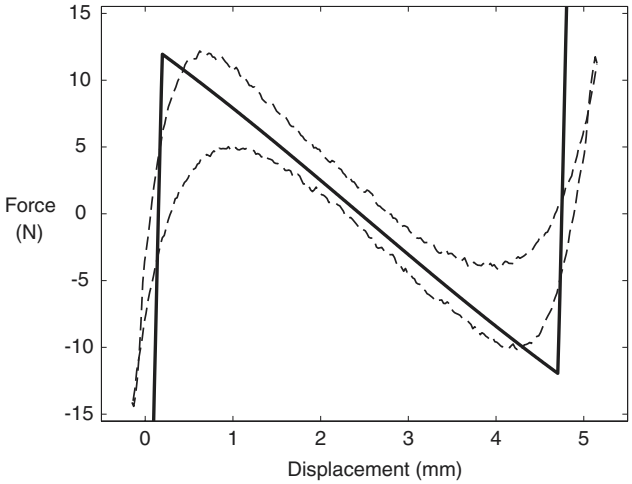

Fig. 20 Comparison of theoretical and experimental behaviour of nylon strut.

Truss Structures

Evaluation of Workspace

In order for a truss architecture to be suitable for a VGT, it must be both statically and kinematically determinate. If this is not the case, the structure will either be a mechanism or it will develop internal states of self-stress whenever any member is actuated. In order to keep production simple, only trusses with repeating units were considered.

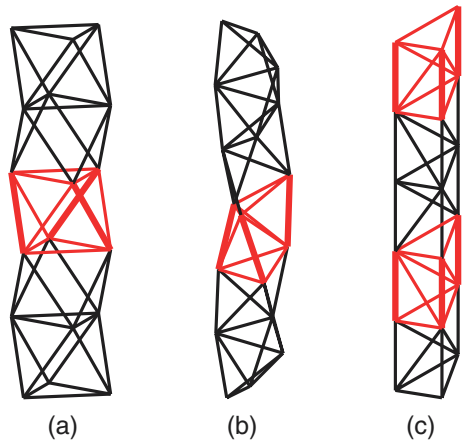

Fig. 21 Three truss structures considered. A unit cell is highlighted in each case. Thicker lines indicate the position of the bistable struts.

Figure 21 shows three of the truss structures considered. In each case, a unit cell is highlighted. Bistable elements were then used to replace three struts in each unit cell. Figure 21(a) shows a truss made up of a number of octahedra. This is a common geometric unit in

space structures. It also has the advantage of having an end element with a normal that is parallel to the axis of the truss. The bistable elements are placed in three of the six elements that connect the triangles that lie in horizontal planes.

Figure 21(b) shows a truss made up of tetrahedra. The highlighted unit cell is made up of three such tetrahedra. The bistable elements are located along the three helices along the edges of this structure.

Figure 21(c) is another tetrahedral truss which has in effect been "untwisted" by extending some of the elements. As this truss form is frequently used in the booms of tower cranes, this truss type will be refereed to as a "crane" truss in the rest of this paper. In each unit cell there is now one element that is $\sqrt{2}$ times longer than all of the other elements. Additionally, every other diagonal bracing element has been rotated by ninety degrees. Hence, two unit cells rather than one have been highlighted. Here, the bistable elements have been located in all of the vertical elements in the truss.

Trusses made up of of ten units of each of the three types of truss shown in Figure 21 were considered. The aim was to find the structure that had the largest possible workspace as well as the most regular distribution of achievable points within the workspace. Having a large workspace is beneficial as it allows the truss to manipulate objects over a larger ares. Having uniformly spaced points is advantageous as it means that inside the workspace a good approximation to any given point is likely to be found.

Due to the relatively short overall length of these structures, their work space is more of an area than a true volume. As the length of the trusses increases, they will be able to bend back on themselves and therefore reach a "volume" of points. If a short truss has the ability to reach a relatively large area it means that it has the ability to exhibit a relatively large curvature. The same functionality is also required for a larger truss to achieve a large work volume.

Each of the three trusses described above incorporates thirty bistable elements and thus each has $2^{30} \approx 1.07 \times 10^9$ unique configurations. Only around ten thousand of these were plotted for each of the trusses. Figure 22 shows these plots superimposed on top of each other. Note that for each of the trusses, the bistable elements were defined as having a length of either 1 or 1.1.

As can be seen from Figure 22, the crane truss appears to give the best spread of points out of the three trusses. It was therefore decided to use this design for the manufacture of a working prototype.

Prototype Truss

A ten unit crane truss was constructed using bistable elements and lightweight polymer tubing. The truss has a total mass of 87 g and a length of 557 mm. Figure 23 shows a picture of the prototype where all of the elements along one side have been actuated. For the purposes of comparison, a picture of the truss modelled in Matlab is also shown. It can be seen that the two shapes correlate well. Note that in this case, the bistable elements have been actuated by hand, rather than by a built-in actuator.

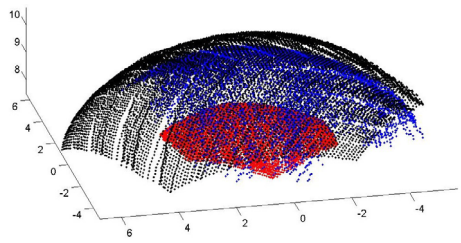

Fig. 22 Workspace of three different trusses: Red = Octahedral truss, Blue = Tetrahedral truss, Black = Crane Truss.

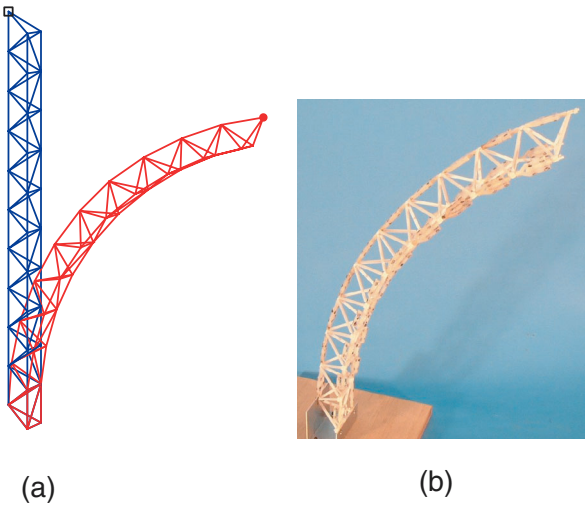

Fig. 23 An actuated state of a multistable truss; (a) Matlab model (red = actuated state, blue = non actuated state); (b) picture of the prototype.

For a more detailed comparison, the predicted horizontal displacement of the truss was 319 mm as opposed to the measured value of 338 mm. Imperfections in manufacturing the model, as well as ignoring gravity effects account for this small discrepancy. What is far more significant is that the prototype displays the expected shape.

Discussion and Conclusions

A novel, bistable structural element based on the snap through properties of a Mises truss has been presented in this paper. A thorough analysis of the buckling of a Mises truss has shown that a simple analysis that accounts for axial compression and Euler buckling of the inclined elements of the snap-through strut has achieved a very good correlation with finite element models. In addition, a good prediction of the

behaviour of a manufactured prototype has been produced.

Based on the simplifying assumptions within which a simple analytical description of the behaviour of the snap-through strut could be obtained, various design graphs have been developed. With these graphs it is possible to obtain preliminary designs for new struts, with different materials and stroke length. Relationships between the snap-through force and various parameters including maximum strain and stroke length have also been developed.

The incorporation of these snap-through elements into several different truss configurations has been investigated. Although by no means exhaustive, our search has shown a "crane" truss found to have good characteristics. A prototype arm was constructed to this design and was found to display the shape characteristics predicted using a Matlab program.

Finally, it should be noted that the study of asymmetric buckling modes presented in this paper did not consider the possibility of the bottom Mises truss moving differently from the upper truss. This type of buckling mode should be further investigated.

Acknowledgments

T.S. thanks the Engineering and Physical Sciences Research Council for the award of a studentship and the Cambridge Newton Trust for additional support. Financial support from Cambridge-MIT Institute (CMI) is gratefully acknowledged.

References

[1]Miura, K., "Variable Geometry Truss Concept", The Institute of Space and Astronautical Science, Report No. 614, 1984.

[2]Rhodes, M. and Mikulas, M.M. Jr., "Deployable Controllable Geometry Truss Beam", NASA Technical Memorandum 86366, 1985.

[3]Pellegrino, S. and Calladine, C.R., "Matrix analysis of statically and kinematically indeterminate frameworks", *International Journal of Solids and Structures*, vol. 22, pp. 409-428, 1986.

[4]Anderson, V.C and Horn, R C., "Tensor Arm Manipulator Design", ASME paper 67-DE-57, 1967.

[5]Roth, B., Rastegar. J. and Scheinman, V., "On the design of Computer Controlled Manipulators", *First CISM-IFTMM Symposium on Theory and practice of Robots and Manipulation*, pp. 93-113, 1973.

[6]Lichter, M., "Concept Development for Lightweight Binary-Actuated Robotic Devices, with Application to Space Systems", *Masters Thesis, submitted to Massachusetts Institute of Technology*, Chapter 2, 2001.

[7]Wingert, A., Lichter, M., Dubowsky, S., and Hafez, M., "Hyper-Redundant Robot Manipulators Actuated by Optimized Binary Dielectric Polymers", *Proceedings of SPIE*, vol. 4695, 2002.

[8]Sudan, V.A., Lichter, M. and Dubowsky, S., "LightweightHyper-redundant Binary Elements for Planetary Exploration Robots", *Proceedings of the 2001 IEEE/ASME International Conference on Advanced Intelligent Mechatronics*, 2001.

[9]Chirikjian, G., "A binary Paradigm for Robotic Manipulators", *Proceedings of IEEE International Conference on Robotics and Automation*, vol. 4, pp 3063-3069, 1994.

[10]Ebert-Uphoff, I., and Chirikjian, G.S., "Inverse Kinematics of Discretely Actuated Hyper-Redundant Manipulators Using Workspace Densities", *Proceedings of the IEEE International Conference on Robotics and Automation*, pp. 139-145, 1996.

[11]Lees, D., and Chirikjian, G.S., "An Efficient Method for Computing the Forward Kinematics of Binary Manipulators", *Proceedings of the IEEE International Conference on Robotics and Automation*, pp. 1012-1017, 1996.

[12]Panovko, Ya.G., and Gubanova, I.I., "Stability and Oscillation of Elastic Systems: Modern Concepts, Paradoxes and Errors", *NASA Technical Translation TT F-751*, 1967, Chapter 2 §5.

[13]Bazant, Z.P., and Cedolin, L., "Stability of Structures", pp. 228-231, Oxford University Press, 1996.